Charge Inversion of a Macroion in Electrolyte Solvent: A Rotating Rod with Polyelectrolyte Counterions

Motohiko Tanaka

National Institute for Fusion Science, Toki 509-5292, Japan

Abstract. Electrophoresis study of charge inversion by molecular dynamics simulation is first reviewed. The cases of spherical and infinite-rod macroions with isolated (spherical) counterions are presented. Then, the charge inversion of a rotating rod macroion of the finite length is examined in the presence of polyelectrolyte counterions. Discrete surface charges (and/or non-smooth surface) are necessary for charge inversion of the rotating rod, which tends to be oriented along the applied electric field due to induced dipole moment. [*International Symposium of Slow Dynamics in Complex Systems (Sendai, Japan, 2003)]*

INTRODUCTION

Charge inversion is the phenomenon principally in electrolyte solvent where each macroion attracts large number of counterions so that the net charge of the aggregates becomes reversed in sign [1, 2, 3, 4, 5, 6, 7, 8, 9, 10, 11, 12]. The charge inversion phenomenon takes place when both of (i) strong electrostatic interactions and (ii) asymmetry in radii and/or valences between counterions and coions, are satisfied [9, 10]. Such conditions are satisfied in high-salt water solutions at room temperature. The phenomenon is not only an interesting physiochemical process in strongly correlated systems, but also has biological applications to the gene therapy as the means of delivering DNAs to living cells [13, 14, 15, 16].

In this article, we first review our electrophoresis study of charge inversion by molecular dynamics simulations [17, 18]. Then, we describe new charge inversion results for a rotating rod of finite length in the presence of polymer (polyelectrolyte) counterions.

Simulation method and parameters are summarized below. The simulation system contains one macroion, many counterions, coions and neutral particles, the last of which represent the solvent. The units of length, charge and mass are, a, e, and m, respectively. Our choice of the temperature corresponds to $a \sim 1.4$Å in water and $m \sim 40$ a.m.u. A macroion with radius $R_0 = 5a$ and negative charge Q_0 is surrounded by the N^+ number of counterions of a positive charge Z^+e and the N^- coions of a negative charge $-Z^-e$. The surface charge density of the macroion is between $\sigma_{sp} = 0.048e/a^2$ (0.39 C/m^2) and $0.26e/a^2$ (2.1 C/m^2). A rod-shaped macroion is also used whose surface charge density is equal to that of DNA, $\sigma_{rod} \approx 0.02e/a^2$ (0.17 C/m^2). The system is maintained in overall charge neutrality, $Q_0 + N^+Z^+e - N^-Z^-e = 0$. The radii of counterions and coions are a^+ and a^-, respectively, with the counterion radius being fixed at $a^+ = a$, and the radius of neutral particles is $a/2$. Approximately one neutral particle is distributed in every volume element $(2.1a)^3 \approx (3\text{Å})^3$ inside the simulation domain, excluding the locations already occupied by ions. These particles are placed in a cubic box of size $L = 32a$, with periodic boundary conditions in all three directions.

The Newton equations of motion are solved for each particle with the Coulombic and Lennard-Jones potential forces under a uniform applied electric field E ($E > 0$),

$$m_i \frac{d\mathbf{v}_i}{dt} = -\nabla\Phi_i(\mathbf{r}_i) + q_i\mathbf{E} \qquad (1)$$
$$\frac{d\mathbf{r}_i}{dt} = \mathbf{v}_i$$

The potential Φ_i is the sum of the Coulombic potential

$$\phi_C = \sum_j q_i q_j / \varepsilon r_{ij} \qquad (2)$$

and the repulsive Lennard-Jones potential which takes care of the volume exclusion effect among particles,

$$\phi_{LJ} = 4\varepsilon_{LJ}[(A/r_{ij})^{12} - (A/r_{ij})^6] \qquad (3)$$

for $r_{ij} = |\mathbf{r}_i - \mathbf{r}_j| \le 2^{1/6}A$, and otherwise $\phi_{LJ} = -\varepsilon_{LJ}$ to exclude the attraction part. Here $\mathbf{r}_i$ is the position vector of the i-th particle, and A is the sum of the radii of two interacting particles.

To account for the periodic boundary conditions for the inverse-square (Coulombic) forces, the Ewald sum

needs to be taken [19]. Numerically, this is accomplished by the particle-particle-particle-mesh (PPPM) method [20, 21]. To treat the rigid-body rotation of the rod macroion in the final section, the Euler equation with the polar coordinates is solved through the quaternion method [22].

We relate ε_{LJ} with the temperature by $\varepsilon_{LJ} = k_B T$, and choose $k_B T = e^2/5\varepsilon a$ (we assume spatially homogeneous dielectric constant ε). The Bjerrum length is thus $\lambda_B = e^2/\varepsilon k_B T = 5a$, which is 7Å in water.

The applied electric field brings in no momentum into the simulation system as it is neutral. However, it does work on the charged particles and heats the solvent through collisions. Thus, it is necessary to drain this Joule heat, and a heat bath is adopted; the macroion is located at the center of the bath at every moment. Although the heat bath generally suppresses long-range interactions, it has no side effects for the present simulation of neutral electrolyte solvent, because the velocity gradients around the macroion are electrostatically screened at short distances [23, 24, 17].

CHARGE INVERSION STUDY BY ELECTROPHORESIS

Charge inversion is the phenomenon that occurs principally without an applied electric field E. Even if the electric field is applied, charge inversion is not affected if the field is weak $E \ll Q_0/\varepsilon R_0^2 \sim 10^6$V/cm. Traditionally, the charge inversion phenomenon has been quantified by two independent criteria, (i) the integrated charge obtained from the radial distribution functions of ions [3, 8, 9, 10, 11], and (ii) the electrophoretic mobility of the macroion [17, 18]. It was found that two criteria agree well except around the threshold for charge inversion [18].

Figure 1 is a bird's-eye view of (a) all the ions and (b) ions in the vicinity of the macroion. Counterions are shown in light gray and coions in dark gray (nearly 4000 solvent neutral particles are not shown) [17]. The macroion has charge $Q_0 = -30e$ and radius $R_0 = 3a$, and counterions are trivalent. The macroion is predominantly covered by the counterions, and coions condense to the topside of the surface counterions because of repulsion from the macroion. Similarly to the case without the electric field [10], the radially integrated charge has a sharp positive peak at a distance about a from the macroion surface. This peak is due to the positive counterions being adsorbed right on the macroion surface. The peak integrated charge for this case is $Q_{\rm peak} \approx 1.6|Q_0|$.

Figure 2 shows the drift speed V_{drift} of the macroion at steady state as a function of the applied electric field E [17]. When the onset conditions are satisfied, the drift speed becomes a linearly increasing function of the (weak) electric field. This means constant electrophoretic mobility $\mu = V_{drift}/E$, and hence, constant net inverted charge $Q^* \sim \nu\mu$, over a wide range of the parameter space (ν the solvent friction). For a very strong electric field comparable to that produced by the bare macroion charge $E \sim Q/\varepsilon R^2$, counterions and coions can no longer stably attach to the macroion. The mobility decreases with the electric field, and flips back to non-reversed [17].

There is a threshold of surface charge density of the macroion σ for charge inversion to take place [17, 18]. Typically, it is $\sigma \sim 0.05e/a^2$ (0.4C/m^2) for a spherical macroion. The corresponding correlation energy of surface counterions is

$$Z^2 e^2/2\varepsilon R_{WS} \sim 5k_B T, \tag{4}$$

where the Wigner-Seitz cell radius $R_{WS} = (Ze/\pi\sigma)^{1/2}$ is half the spacing between the surface counterions. The reversed mobility increases either with ionic strength and/or valence of counterions for small ionic strength and/or valence.

The asymmetry of radii and/or valences between counterions and coions causes or enhances charge inversion. Figure 3 shows the dependence of the reversed mobility against the ratio of coion to counterion radii a^-/a^+. (The normalization is $\mu_0 = \nu_0/(|Q_0|/\varepsilon R_0^2) \approx 21(\mu\text{m/sec})/(\text{V/cm})$ with ν_0 the thermal speed of neutral particles.) With the ratio of the radii, the mobility increases linearly up to $a^-/a^+ \leq 1.5$. This is because coions with larger size geometrically compete with each other to condense on the surface counterions, which is consistent with Monte Carlo simulations of charge inversion of the finite-size coions [25] and the condensation of the $Z:1$ ions with the size asymmetry [26].

Large asymmetry of valences also causes charge inversion. In Fig.4, (reversed) mobility is plotted against the interaction energy of counterions and coions $Z^-Z^+e^2/2\varepsilon\gamma a$. Here, counterions are either divalent, trivalent or tetravalent, and coion valence ranges from unity to five; the asymmetry becomes larger on the left-hand side of the figure [18]. Interestingly, mobilities for different valences, Z^+ and Z^-, collapse to a master curve whose index is the interaction energy. Here, the γ factor stands for screening by coion condensation onto the surface counterions, which is a general feature of charge inversion, as seen in Fig.1.

At small ionic strength, the monovalent salt enhances reversed mobility of a strongly charged macroion, as shown with filled squares in Fig.5 [18]. Monovalent salt ions fill the vacancies on the macroion not occupied by multivalent counterions due to repulsion among them. The electrostatic energy of the whole system is thereby globally minimized. It is quite remarkable that, even

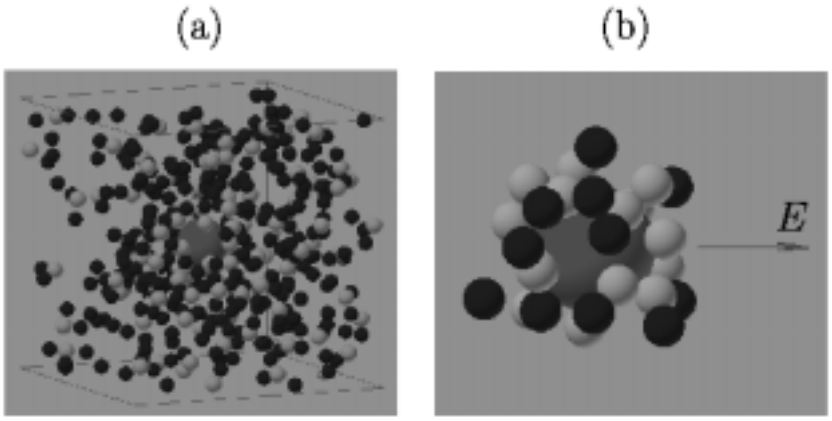

FIGURE 1. Bird's-eye view of (a) all the ions in the simulation domain and (b) the screening ion atmosphere within $3a$ from the macroion surface. A macroion with charge $Q_0 = -30e$ and radius $R_0 = 3a$ is a large sphere located in the middle; trivalent counterions and monovalent coions are shown by light and dark gray spheres, respectively. The arrow to the right shows the direction of the electric field (x-axis), with $E = 0.3\varepsilon/ea$.

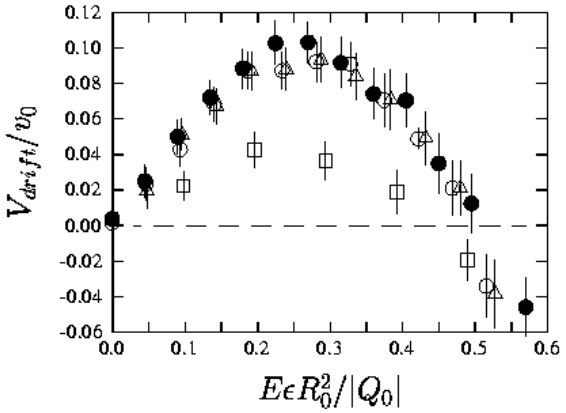

FIGURE 2. Dependence of the macroion drift speed V_{drift} (v_0: the thermal speed of solvent particles) on the electric field E for a macroion of various radii and charges. Counterions are trivalent and the Bjerrum length is $\lambda_B = e^2/\varepsilon k_B T = 5a$ where a is the radius of counterions.

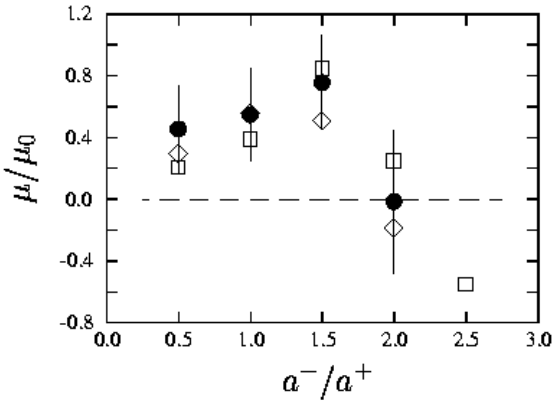

FIGURE 3. The electrophoretic mobility of the macroion μ against the ratio of coion and counterion radii a^-/a^+. Counterions are divalent (diamonds), trivalent (circles), and pentavalent (squares) with radius $a^+ = a$. The macroion radius is $R_0 = 5a$ and surface charge density $\sigma_{sp} \sim 0.26e/a^2$ (2.1 C/m^2). The Bjerrum length is $\lambda_B = 5a$.

for the case where excess counterions are not present, $Q_0 + eZ^+N^+ = 0$, charge inversion is invoked by the addition of monovalent salt when the macroion is strongly charged (open squares). Coexistence of multivalent and monovalent counterions should be energetically more favorable to achieve charge inversion. On the other hand, either at large ionic strength or for a weakly charged macroion (filled square), monovalent salt simply screens and suppresses charge inversion.

An infinite rod macroion shows similar but somewhat different dependences on the monovalent salt. Two different settings are compared: (i) a cylindrical macroion with polyelectrolyte counterions and (ii) a spherical macroion with isolated counterions, for the same surface charge densities. (The rod moves in the (x,z) space with its axis oriented perpendicularly to the applied electric field, which should give rise to maximum mobility compared to a rotating rod.) At zero salt, they both have the same mobility, while for finite ionic strength the former is more persistent to added monovalent salt than the latter [18]. Furthermore, it was demonstrated that the mobility of an elongated macroion can be reversed or enhanced by mechanical twining of polyelectrolyte counterions around the rod axis [27]. These findings support the advantage of using polyelectrolyte counterions such

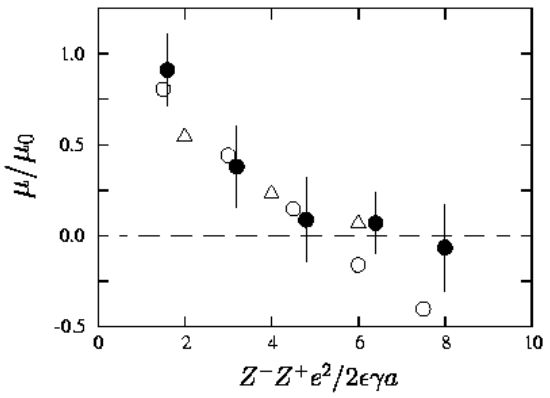

FIGURE 4. The macroion mobility is shown against the interaction energy of counterions and coions $Z^+Z^-e^2/2\varepsilon\gamma a$, for the fixed counterion valences, $Z^+ = 2$ (triangles), $Z^+ = 3$ (open circles), and $Z^+ = 4$ (solid circles). The γ factor is 1.0, 2.0 and 2.5 for $Z^+ = 2$, 3 and 4, respectively. Coions and counterions are of the same radius, $a^- = a^+ = a$, and the temperature is $e^2/\varepsilon a k_B T = 5$.

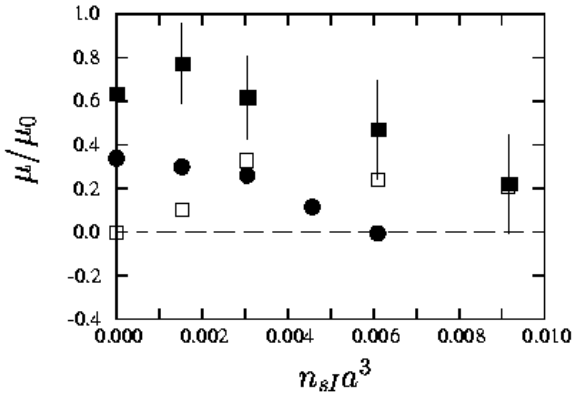

FIGURE 5. The electrophoretic mobility of the spherical macroion is shown against ionic strength of monovalent salt n_{sI} (1 Mol/l salt corresponds to $0.0017/a^3$). The surface charge density of the macroion is $\sigma_{sp} = Q_0/4\pi R_0^2 \sim 0.26e/a^2$, with excess Z-ions (filled squares), and without excess Z-ions (open squares). Also, the mobility for the macroion $\sigma_{sp} \sim 0.080e/a^2$ with excess Z-ions (filled circles) is shown. Here, $\mu_0 \approx 21(\mu\mathrm{m/sec})/(\mathrm{V/cm})$.

as spermidine and spermine in charge inversion of biological matters including DNA.

ROTATING ROD OF FINITE LENGTH

The charge inversion of an infinite rod macroion was studied by molecular dynamics simulations [28, 18]. The effect of finite length was examined for a static (perpendicular) rod previously [18]. It was shown that the rod length ℓ does not affect the mobility if $\ell/R \geq 3$ (R: the rod radius). In the below, a macroion is a finite-length rod ($\ell = 16a$, $R = 4a$) that can rotate as a rigid body. The macroion charge $Q_{rod} = -14e$ is provided by localized discrete unit charges aligned on the double helices, which are shown with white spheres in Fig.6. The average surface charge density is chosen equal to that of the DNA $\sigma_{DNA} \sim 0.023e/a^2$ (0.19 C/m^2), and the initial rod axis is placed perpendicularly to the electric field ($\Theta = 90°$). The number of coions is nearly fixed $N^- = 31$, which determines that of counterions by charge neutrality. Coion radius is larger than that of counterions, $a^- = 1.5a^+$. The applied electric field is weak compared to the self electric field produced by the rod macroion, $E_{rod} \sim Q/2\pi R\ell$, so that the electrophoresis occurs well in the linear regime of Fig.1.

When the counterions are made of polyelectrolyte, where each chain consists of three trivalent monomers $3e - 3e - 3e$, the peak integrated charge far exceeds bare macroion charge in the top panel of Fig.8(a), $Q_{peak}/|Q_0| \sim 2.5$, implying strong adsorption of polyelectrolyte counterions to the macroion, and therefore charge inversion. This is verified in the radial distribution functions (RDF) of Fig.7(a), which depicts the charge densities of counterions (open bars) and coions (shaded bars), and that of the integrated charge (inset panel). Also in the dynamical criterion, the mobility of the macroion is reversed on time average, as seen for the drift speed in the bottom panel of Fig.8(a).

The angle Θ between the rod axis and the electric field in the middle panel of Fig.8(a) shows that the rod axis tends to be oriented parallel to the electric field, similarly with the case of a very strong electric field [29]. This arises from minimization of the electrostatic energy for the macroion with the induced dipole moment due to adsorbed counterions and coions. Namely, more positive (negative) ions tend to stay at the positive (negative)-x side of the rod which rotates the rod if it is not aligned parallel to the applied electric field. The dipole moment along the rod axis is measured. For the instantaneous value, large fluctuations preclude the detection of the dipole moment. However, the time integration clearly shows the buildup of the constant and negative dipole moment pointing along the rod axis, whose time history is closely analogous to that of the rod angle in the middle panel of Fig.8(a).

We note in passing that, for the rotating rod, the surface charge of the macroion needs to be localized and discrete to pin down the counterions. Otherwise for the uniform surface charge and the smooth cylinder, the counterions and coions slip on the macroion surface and easily desorbed from the tips of the rod. This strongly suggests the importance of the actual non-smooth surface of the macroion such as the DNA, which is characterized by side groups branches and specific *ion traps*.

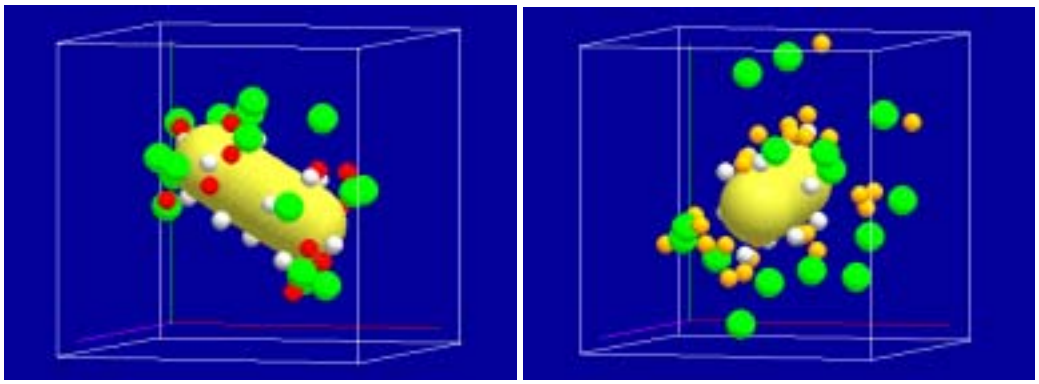

FIGURE 6. The bird's-eye view of the rotating rod macroion of the finite axis-length corresponding to the runs in Fig.8(a) (left) and Fig.8(b) (right). Discrete macroion surface charges (unit charge e) are shown with white spheres, counterions with dark gray spheres and coions with large spheres. The applied electric field points rightward along the box edge.

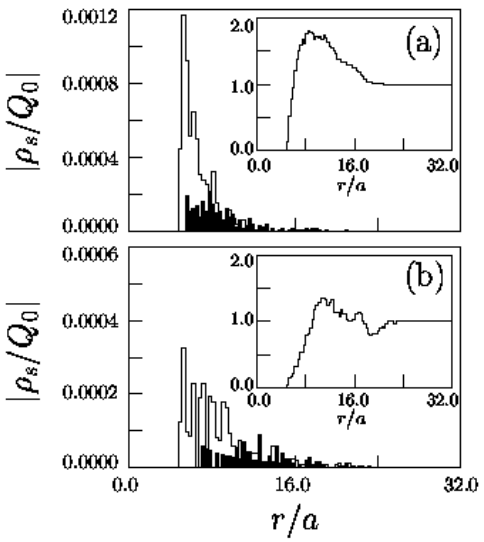

FIGURE 7. Radial distribution functions of charge density of counterions (open bars) and coions (shaded bars), and the integrated charge (inset panel) for the rod macroions in Fig.8. The finite-length rod macroion is put in the solution of polyelectrolyte counterions, each chain of which consists of three (a) trivalent, and (b) monovalent monomers.

Indeed, the inclusion of the attractive Lennard-Jones potential $\varepsilon_{LJ} = k_B T$ in the molecular dynamics simulation makes the mobility reversed for the rod macroion with DNA's surface charge density [27].

On the other hand, for the polyelectrolyte counterions consisting of all unit charges $e-e-e$ with other conditions fixed, the mobility is not reversed. The adsorption of counterions to the very surface of the macroion is not significant either, as seen in Fig.6(b), which is just around the charge neutralization level $Q_{peak}/|Q_0| \sim 1$ (see Fig.8(b)). In this case, the rod does not rotate but stays around the initial angle. Although the RDF of the integrated charge in Fig.7(b) (inset panel) is peaked above neutrality, it is associated with an overshoot to below unity after the primary peak. The macroion with this type of the RDF in *charge inversion* usually shows non-reversed mobility, including the case of spherical macroions [18].

ACKNOWLEDGMENTS

It is a great pleasure of the author to thank Prof. A.Yu.Grosberg for a series of close collaborations on molecular dynamics study of charge inversion. This work was supported by the Grant-in-Aid No.15035218 (2003) from the Ministry of Education, Science and Culture of Japan. The computation was performed mainly with the supercomputers of the University of Minnesota Supercomputing Institute.

REFERENCES

1. Grosberg, A.Yu., Nguyen, T., and Shklovskii, B., *Reviews Modern Phys.*, **74**, 329–345 (2002).
2. Quesada-Perez, M., Gonzalez-Tovar, E., Martin-Molina, A., Lozada-Cassou, M., and Hidalgo-Alvarez, R., *ChemPhysChem.*, **4**, 234–248 (2003).
3. Gonzales-Tovar, E., Lozada-Cassou, M., and Henderson, D.J., *J. Chem.Phys.*, **83**, 361–372 (1985).
4. Elimelech, M., and O'Melia, C.R., *Colloids Surface*, **44**, 165–178 (1990).
5. Bastos, D., and De Las Nieves, F.S., *Colloid Poly. Sci.*, **271**, 860–867 (1993).
6. Walker, H.W., and Grant, S.B., *Colloids Surfaces*, **A119**, 229–239 (1996).
7. Netz, R.R. and Joanny, J.F., *Macromolecules*, **32**, 9013–9026 (1999).

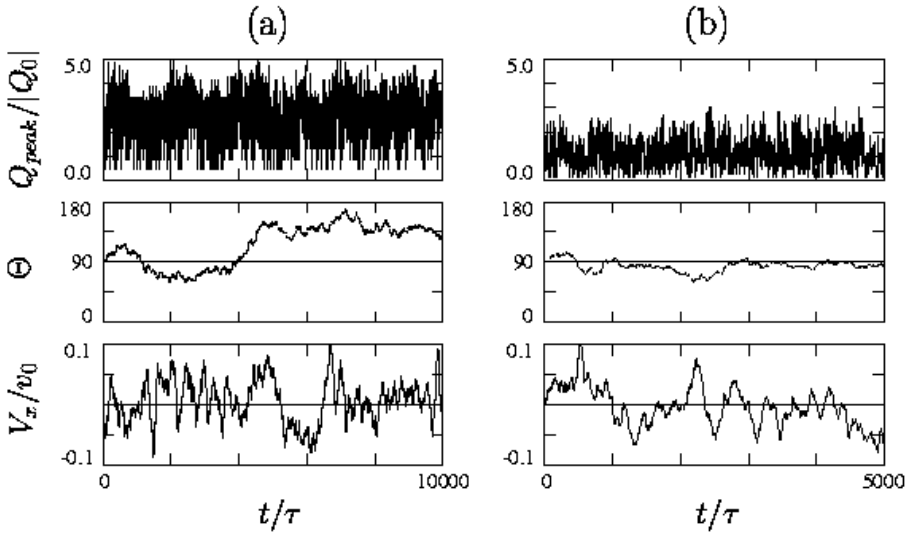

FIGURE 8. Time histories of the integrated peak charge Q_{peak}, the angle between the rod axis and the electric field Θ, and the drift speed of the macroion V_x, from top to bottom. The macroion is the finite-length rotating rod shown in Fig.6, the counterions are polyelectrolyte, each of which is a chain of three (a) *trivalent* and (b) *monovalent* counterions, and the coions are spheres of large radius. The surface charge density of the macroion is chosen the same as that of the DNA, which is provided by localized discrete unit charges aligning along double helices on the rod. The electric field is weak, (a) $E = 0.02\varepsilon/ea$ and (b) $E = 0.005\varepsilon/ea$. The time normalization is $\tau \approx 1$ ps.

8. Nguyen, T., Grosberg, A.Yu., and Shklovskii, B.I., *Phys.Rev.Lett.*, **85**, 1568–1571 (2000).
9. Messina, R., Holm, C., and Kremer, K., *Phys.Rev. Lett.*, **85**, 872–875 (2000).
10. Tanaka, M., and Grosberg, A.Yu., *J.Chem.Phys.*, **115**, 567–574 (2001).
11. Lozada-Cassou, M., and Gonzales-Tovar, E., *J. Colloid Interf.Sci.* **239**, 285–295 (2001).
12. Levin, Y., *Rep.Prog.Phys.*, **65**, 1577–1632 (2002).
13. Sukhishvili, S.A., Obolskii, O.L., Astafieva, L.V., Kabanov, A.V., and Yaroslavov, A.A., *Vysokomol.Soed.*, **35**, 1895–1899 (1993) [*Polymer Sci.*, **A35**, 1895–1899 (1993).]
14. Kabanov, A.V., and Kabanov, V.A., *Bioconj.Chem.*, **6**, 7–20 (1995).
15. Gelbart, W.R., Bruinsma, R., Pincus, P., and Parsegian, A., *Physics Today*, **53**, 38-44 (2000).
16. Ewert, K., Ahmad, A., Evans, H.M., Schmidt, H.W., and Safinya, C.R., *J.Med.Chem.*, **45**, 5023–5029 (2002).
17. Tanaka, M., and Grosberg, A.Yu., *Euro.Phys.J.*, **E7**, 371–379 (2002).
18. Tanaka, M., *Phys.Rev.E*, **68**, 061501 (2003).
19. Ewald, P.P., *Ann.Physik*, **64**, 253–287 (1921).
20. Eastwood, J.W., and Hockney, R.W., *J.Comput.Phys.*, **16**, 342–359 (1974).
21. Deserno, M., and Holm, C., *J.Chem.Phys.*, **109**, 7678–7693 (1998).
22. Evans, D.J., *Mol.Phys.*, **34**, 317–325 (1977).
23. Long, D., Viovy, J.-L., and Ajdari, A., *Phys.Rev.Lett.*, **76**, 3858–3861 (1996).
24. Viovy, J.-L., *Rev.Mod.Phys.*, **72**, 813–872 (2000).
25. Greberg, H., and Kjellander, R., *J.Chem.Phys.*, **108**, 2940–2953 (1998).
26. Panagiotopoulos, A.Z., and Fisher, M.E., *Phys.Rev.Lett.*, **88**, 045701 (2002).
27. Tanaka, M., *J.Phys.: Condensed Matters* (submitted) (2003); *cond-mat* /0311009 (2003).
28. Deserno, M., Jimenez-Angeles, F., Holm, C., and Lozada-Cassou, M., *J.Phys.Chem.*, **B105**, 10983–10991 (2001).
29. Netz, R.R., *Phys.Rev.Lett.* **90**, 128104 (2003).